RSC Advances

PAPER

Cite this: *RSC Adv.*, 2015, **5**, 41285

Production of gamma-valerolactone from sugarcane bagasse over TiO_2-supported platinum and acid-activated bentonite as a co-catalyst

Jindrayani N. Putro,[a] Alfin Kurniawan,[b] Felycia E. Soetaredjo,*[a] Shi-Yow Lin,[b] Yi-Hsu Ju[b] and Suryadi Ismadji*[a]

Nowadays, biomass utilization has become the center of attention for researchers worldwide and is driven by the depletion of global petroleum supplies for the production of energy and valuable chemicals while easing the atmospheric CO_2 burden. We propose here a green strategy for transforming sugarcane bagasse into gamma-valerolactone (GVL), an attractive platform molecule that can be further converted into a variety of chemical derivatives for wide use in industrial applications. Our recent strategy involves the solid acid-catalyzed hydrothermal conversion of cellulose and hemicellulose derived from biomass to give an aqueous solution comprising levulinic acid (LA), followed by catalytic hydrogenation of LA to GVL. Native and acid-activated bentonites were used as solid acid catalysts to promote hydrothermal conversion of cellulose and hemicellulose. The maximum achievable yield of LA was 159.17 mg per gram of oven-dried biomass for 60 min reaction at 473.2 K in the presence of a 2% acid-activated bentonite catalyst. Catalytic hydrogenation reactions of LA to GVL over 1% Pt@TiO_2 and acid-activated bentonite as a co-catalyst were performed at temperatures of 393.2–473.2 K and residence times of 120–360 min. The combined solid catalyst gave an attractive performance with respect to LA conversion (~100%) and GVL selectivity (95%) under milder reaction conditions in comparison to 1% Pt@TiO_2 without an acid co-catalyst. The spent catalyst could be reused for five consecutive hydrogenation cycles with a marginal decrease in the catalytic activity and GVL selectivity. Coke formation was believed to be the main cause of catalyst poisoning and calcination of the spent catalyst under a stream of pure oxygen at 723.2 K was applied for removing coke deposits from the active catalyst sites, thus restoring the catalytic performance.

Received 7th April 2015
Accepted 30th April 2015

DOI: 10.1039/c5ra06180f

www.rsc.org/advances

Introduction

Over the past decade, the 2nd generation of liquid biofuels has become the present global challenge in the energy field. The primary focus of such research is to develop sustainable liquid biofuels from lignocellulosic biomass in a competitive market and environmentally sustainable route, which can be used to replace finite fossil fuel resources and boost the economics of biofuel production.[1,2] Lignocellulosic biomass, in the form of agricultural crops, forestry residues or waste from whole food supply chains is being paid more attention worldwide as a potential resource for the production of liquid biofuels, thanks to its renewability, high abundance and inherently carbon neutral nature.[3–5] Lignocellulosic biomass consists of 35–50% cellulose, 20–35% hemicellulose and 10–25% lignin.[5] All are natural polymeric materials which constitute the structural integrity and much of the mass of plants. The challenge now is to find an alternative route to convert the hardly decomposed cellulose and hemicellulose into five- and six-carbon sugars that can be run economically at the scale required. The existing thermochemical routes which are considered more economically and technically feasible than conventional biochemical route featuring enzymatic hydrolysis and fermentation for the conversion of lignocellulosic biomass to fuels and commodity chemicals include the Fischer–Tropsch synthesis (FTS) and biofine processes, catalytic hydrotreatment, catalytic pyrolysis and hydrothermal liquefaction.[5–11] However, one the major obstacles faced in these thermochemical conversion routes is associated with the production of bio-crude containing high oxygen, nitrogen and sulfur, which renders the product with undesirable properties as fuel including thermally and chemically unstable, corrosive and low energy density. Further physical or chemical upgrading strategies are required in order to improve the quality of as-produced biocrude, which often involves a series of unit operations and extensive energy input requirements for the processes performed under high temperature conditions. Furthermore, the implementation of most, if not all, of the aforesaid thermochemical technologies for industrial process scale-up is now under-performing.

[a]*Department of Chemical Engineering, Widya Mandala Surabaya Catholic University, Kalijudan 37, Surabaya 60114, Indonesia. E-mail: suryadiismadji@yahoo.com*
[b]*Department of Chemical Engineering, National Taiwan University of Science and Technology, No. 43, Sec. 4, Keelung Rd, Taipei 106, Taiwan, Republic of China*

There are two critical steps in the conversion of cellulosic components of lignocellulosic biomass into fuels and chemicals: hydrolysis and dehydration processes. In the hydrolysis process, hemicellulose is converted into five- and six-carbon sugars under catalysis by mineral acids (mostly sulfuric acid) while cellulose fiber is enzymatically hydrolyzed into glucose by commercial cellulase and cellobiase enzymes. The resulting aqueous mixture of fermentable sugars containing xylose, arabinose and glucose then undergoes dehydration reaction, leading to formation of levulinic acid (LA) and furan derivatives. In the next process, the aqueous solution containing LA undergoes catalytic reduction with molecular hydrogen to form gamma-valerolactone (GVL), which serves as a high-value chemical intermediate for the production of straight and branched alkanes and cycloalkanes with appropriate molecular weight and structure for use in gasoline and jet fuel applications. Intensive research activities have sought to develop a simple yet highly efficient catalyst for the hydrogenation of LA to GVL. Heterogeneous catalysts based on noble metals such as Pd, Ru, Rh, Pt, Au and Ir and base metals such as Fe, Cu, Co and Ni on carbon, zeolite or metal oxide support materials have received much attention for practical use,[8,10,12–18] mainly associated with their advantages such as ease of catalyst separation, reusability, less damage to reactor and relatively high turnover numbers (TONs). Homogeneous catalytic systems have also shown great potential for the hydrogenation of LA to GVL in terms of catalyst activity and selectively under relatively mild reaction conditions. For instance, ruthenium/phosphine complexes, especially complexes with the facially coordinating tridentate ligand (TriPhos) have found application as a highly active catalyst toward carbonyl compounds such as esters and amides and even free carboxylic acids in the homogeneous hydrogenation reaction.[19] Robust iridium trihydride complexes of pincer ligands with TONs as high as 71 000 have been tested for the synthesis of GVL from hydrogenation of biomass-derived LA under relatively mild reaction conditions by Zhou and his group[20] and the GVL yield could reach 99%. Very recently, Tukacs and co-workers have reported the application of ruthenium catalysts modified with bidentate phosphine ligands and they showed that the proposed catalytic system could be reused for ten consecutive runs while achieving full conversion of LA with a representative turnover frequency (TOF) of 21 233 h^{-1} in solvent-, chlorine- and additive-free reaction environments.[21] GVL has proved to demonstrate many of the important properties of an ideal liquid fuel including renewable, easy and safe to store and transport, very low vapor pressure even at high temperature (3.5 kPa at 80 °C), high boiling point (207 °C) and open cup flash point (96 °C) and miscible with water.[22] Therefore, the production of GVL from lignocellulosic biomass has moved globally in large numbers and very recent potential applications include a green reaction medium for the conversion of various carbohydrates to 5-hydroxymethylfurfural (5-HMF) and LA,[22,23] ionic liquid phase catalytic system for the hydrogenation of different olefins,[24] precursors in manufacturing bio-based polymers and resins[25] or chemical additives for gasoline and diesel fuel.[23]

Sugarcane bagasse (SB) is a major agro-industrial byproduct generated from the sugar milling. In the sugar milling process, a part of this fibrous residue is normally burned to generate steam and electricity for factory operation and stockpiling becomes a common practice for handling the excess bagasse. However, long-term storage of large quantities of bagasse in the uncovered stockpiles continues to be a menace to the environment and surrounding communities through hazards associated with spontaneous combustion, groundwater seepage and generation of contaminated leachates. It is required to find a suitable use for the excess bagasse as a means of managing these hazards and minimizing potential environmental impacts. SB is composed of cellulose, hemicellulose and lignin and more importantly this lignocellulosic biomass has significant advantage that it does not interfere with food resources for chemicals and fuels production. Several studies[22,23,26] have demonstrated different methods for transforming sugars in lignocellulosic biomass into sustainable platform chemicals such as LA, GVL and furanic aldehydes (*e.g.*, 5-HMF and furfural). For instance, the high sugar-containing juice derived from sweet sorghum can be utilized as a non-food source to produce platform molecules namely LA and 5-HMF by a microwave dielectric heating method.[27] The maximum yield of LA (31.4%) was achieved from the sorghum sample treated for 20 min centrifugation time in the presence of 2 M sulfuric acid under 30 min microwave irradiation. Horvath and co-workers[28] investigated several intermediates and different reaction pathways in the acid-catalyzed dehydration of fructose to 5-HMF in dimethyl sulfoxide solvent with or without sulfuric acid as catalyst. They found from isotopic labeling results that the reversible formation of 2,6-anhydro-β-D-fructofuranose intermediate played a crucial role in controlling two irreversible pathways toward desirable product (5-HMF) *via* a furanose route or toward the unwanted side products *via* a pyranose route. In this study, we utilize non-food SB biomass as a potential raw material for the production of GVL *via* a two-step process involving a first step for hydrothermal conversion of biomass to LA and a second step for hydrogenation of LA to GVL. In the first step, subcritical water (hereafter called sub-CW) is used as a reaction medium, which is safe, non-toxic, inexpensive and readily available. The native and acid-activated bentonites are used as heterogeneous solid acid catalysts in the first step and the catalyst performance study for given reaction is presented. On the other hand, titania-supported platinum catalysts ($Pt@TiO_2$) in the absence or in combination with acid-activated bentonite as a co-catalyst are utilized in the second step. The catalyst performance evaluation in the second step is based on LA conversion, GVL selectivity and GVL yield. Furthermore, the effects of temperature and residence time on the extent of hydrogenation of LA to GVL are investigated and discussed in this paper. Finally, studies were carried out to assess the potential reuse of the hydrogenating catalyst in at least five consecutive reaction cycles.

Experimental

Materials

SB was collected from a cane sugar mill located at Klaten district in Central Java. The collected biomass was repeatedly washed with tap water to remove surface impurities and dried in an

oven at 80 °C for 12 h. The dried biomass was pulverized using a bench-scale hammer mill to particle sizes ranging from 0.15–0.18 mm (80/100 mesh, U.S. Sieve Series). Moisture content of the pulverized biomass was determined by using an Ohaus® MB-35 moisture analyzer. Delignification step was conducted by soaking powdered biomass into a 20 wt% sodium hydroxide solution with a solid to solution ratio of 1 : 10 under continuous stirring (500 rpm) at room temperature for 24 h. The treated biomass was separated by vacuum filtration, washed with warm distilled water until the pH of the washing solution ranged between 6.5 and 7 and oven-dried at 110 °C for 12 h. The final product (DSB) was stored in sealed plastic bags for further use. The determination of lignocellulose contents of SB and DSB samples was carried out following the standardized wet chemical methods used in the wood industry sector. The percentage weights of the elements C, H, N, O and S of SB and DSB samples were determined by a CHNS/O analyzer model 2400 from Perkin-Elmer. The proximate analysis was conducted following the established ASTM procedure. The results from three repeated analyses are presented as average values ± standard deviations (Table 1).

Natural Ca-bentonite with grayish white color was collected from a mining site located at Pacitan district in East Java. Prior to its use, the bentonite was purified according to the procedure described by Soetaredjo and colleagues.[29] The chemical composition of the purified bentonite was SiO_2 (63.5%), Al_2O_3 (17.8%), Fe_2O_3 (2.2%), MnO_2 (0.5%), TiO_2 (0.2%), MgO (1.2%), K_2O (1.6%), Na_2O (1.5%), CaO (2.8%) and LOI (loss on ignition) (8.7%). The montmorillonite content of the bentonite was 78%. Anatase titanium(IV) oxide (TiO_2) powder (99%) was purchased from Sigma Aldrich, Singapore and used as-received. For chemical analysis and preparation of catalysts, the following reagents include anhydrous sodium hydroxide pellets (98%, Sigma Aldrich), sulfuric acid (98%, Merck), chloroplatinic acid hexahydrate (8 wt% in H_2O, Aldrich), acetonitrile (LC-MS CHROMASOLV®, 99.9%, Fluka), hexyl alcohol (99.9%, Fluka) and standards of D(+)glucose (99.5%, Sigma), D(+)xylose (99%, Aldrich), L(+)arabinose (98%, Aldrich), D(+)galactose (99%, Fluka), furfural (98.5%, Fluka), 5-HMF (98%, Fluka), LA (98%, Aldrich) and GVL (98.5%, Fluka) were directly used without further purification. Ultra-high purity nitrogen and hydrogen gases (99.9%) were supplied by a local company. The ultrapure water obtained from a Milli-Q water filtration station (Millipore Corp., Milford, MA) was used in all experiments unless otherwise stated.

Table 1 Characteristics of SB and DSB lignocellulosic materials

Components	SB	DSB
Hemicellulose	24.7 ± 2.5	18.8 ± 0.9
Cellulose	35.4 ± 1.8	52.7 ± 2.1
Lignin	21.8 ± 1.2	10.3 ± 0.8
Ultimate compositions, wt% (on dry basis)		
Carbon	53.2	53.8
Hydrogen	6.1	6.2
Nitrogen	0.5	0.6
Sulphur	1.8	1.7
Oxygen (by difference)	38.4	37.7
Proximate compositions, wt% (on dry basis)		
Volatile matter	66.1 ± 2.4	64.8 ± 1.7
Fixed carbon	15.8 ± 0.5	17.0 ± 1.2
Moisture content	5.9 ± 0.7	6.5 ± 0.3
Ash content	12.2 ± 1.2	11.7 ± 0.7
Sugar compositions, mg g^{-1} (on dry basis)		
Glucan	348.7 ± 5.9	507.8 ± 2.7
Xylan	216.0 ± 4.4	165.6 ± 3.5
Galactan	2.5 ± 0.3	1.9 ± 0.2
Arabinan	27.6 ± 2.5	20.1 ± 1.3

Preparation of catalyst materials

Natural Ca-bentonite was utilized as a heterogeneous solid catalyst in this study due to its mechanical and hydrothermal stability, low swelling capacity, high cation exchange capacity (CEC, 58.3 meq. 100 g^{-1} clay according to methylene blue test method designed in ASTM C837-99), environmentally benign and easily obtainable material. The acid treatment of bentonite aims to enhance its adsorption and catalytic properties for the hydrolysis of cellulosic components of biomass into water-soluble saccharides. The acid-activated bentonite was prepared based on the following procedure: 50 g of purified bentonite was immersed in a 500 ml solution of sulfuric acid (2 N) and transferred into a round-bottom flask. The resulting suspension was heated at 80 °C under reflux and stirring for 4 h. Then, the solid was separated by vacuum filtration, washed with warm distilled water until free of sulphate ions (tested by $BaCl_2$ solution) and dried in an oven at 110 °C for 6 h. The acid-activated bentonite was crushed and sieved to particle sizes of 125–150 μm. Here, the untreated and acid-activated bentonite samples were designated as UB and AAB, respectively. The titania-supported 1 wt% Pt catalyst (1% Pt@TiO_2) was prepared by incipient wetness impregnation method based on Zhang and co-workers procedure.[30]

Characterizations of biomass precursors and catalyst materials

The thermal stability of SB and DSB samples was determined by thermal gravimetric analysis (TGA) using a Mettler-Toledo TGA/DTA 1 thermal analyzer with a heating and cooling rate of 10 K min^{-1} up to 1073 K under continuous nitrogen gas flow of 150 ml min^{-1}. The mass of the samples in each experiment was about 10 mg. The surface morphology of biomass precursors and catalyst materials was visualized by scanning electron microscope (SEM), on a JEOL JSM-6390F operated at an accelerating voltage of 10 kV. Prior to SEM imaging, an ultra-thin layer of conductive platinum was sputter-coated on the specimens using an auto fine coater (JFC-1200, JEOL, Ltd., Japan) for 120 s in an argon atmosphere. The powder X-ray diffraction (XRD) patterns were acquired on a Philips PANalytical X'Pert powder X-ray diffractometer with a monochromated high-intensity Cu $K\alpha_1$ radiation (λ = 0.15406 nm) operating at 40 kV, 30 mA and a step size of 0.05° s^{-1} in the 2-theta scan range of 5–90°. The peak locations corresponding to the

crystalline phases were compared with standard JCPDS files. The specific surface areas and pore structures of the catalysts were characterized by nitrogen adsorption–desorption isotherms. The adsorption and desorption isotherms were conducted at the boiling temperature of liquid nitrogen (77.2 K) using an automated Micromeritics ASAP2010 sorption apparatus. Before measurements, the samples were outgassed under vacuum for 6 h at 473.2 K. The Brunauer–Emmett–Teller (BET) equation was used to calculate the specific surface area from adsorption data in the relative pressure (P/P^o) range of 0.01–0.30. Total pore volume (V_T) was determined from the amount of adsorbed gas at a relative pressure of 0.995.

Catalytic hydrothermal conversion of DSB biomass

The hydrothermal conversion of DSB biomass was carried out in a 150 ml lab-scale high pressure batch reactor. The high pressure batch reactor was equipped with a pressure gauge, an external electrical heating system, a Type K thermocouple as internal temperature control device and M8 screws for tightening the reactor with its cap. The maximum allowable operating pressure and temperature of the reactor are 10 MPa and 523.2 K, respectively. Typical hydrothermal conditions were described as follows: temperatures 393.2–473.2 K, catalyst loading 0–2% (w/v), DSB to water ratio 1 : 10 (w/v), stirring speed (300 rpm) and internal pressures (3–5 MPa). The hydrothermal reaction was conducted at desired temperatures for 60 min and after the completion of reaction, the reactor was rapidly cooled down to room temperature by quenching in a cold water bath and the gas pressure was recorded and vented. The solid fraction was separated by centrifugation at 3000 rpm for 15 min. An aliquot of liquid samples obtained after the reaction was withdrawn and the concentrations of 5-HMF, furfural, LA, organic acids and monomeric sugars were quantified by using high performance liquid chromatography (HPLC) as described later.

Catalytic hydrogenation of hydrothermal liquor containing LA

The catalytic hydrogenation reactions were performed in a 250 ml Parr 4576A bench top stirred HP/HT reactor equipped with a temperature controller unit (model P.I.D. 4843), a pressure transducer and gage and overhead stirring. Before use, the catalyst was activated under flowing H_2 at 573.2 K and atmospheric pressure for 3 h. In a typical procedure, the aqueous solution containing LA obtained from hydrothermal reaction at 453.2 K with 2% AAB catalyst was introduced into the reactor, followed by the addition of 0.5 g of catalyst comprising 0.4 g 1% Pt@TiO_2 and 0.1 g AAB as an acid co-catalyst. An equivalent amount of 1% Pt@TiO_2 hydrogenation catalyst (0.4 g) was also used in the reaction. In order to remove air inside the reaction vessel, the reactor was slowly flushed with argon three times before hydrogen gas was charged. Afterward, the reactor was pressurized with hydrogen gas to 3 MPa and sufficient temperature ramping time was allowed before the reaction step at the chosen temperature. Zero reaction time was defined when the temperature inside the reactor reached the chosen temperature. The hydrogenation reactions were performed at temperatures of 393.2–473.2 K and residence times were varied between 120 and 360 min. During the course of the reaction, mixing was achieved through an internal 4-blade impeller operating at 1200 rpm. Preliminary experiments showed that this stirring speed was sufficient to avoid external mass transfer limitation, thus ensuring the reaction operates in the kinetic regime. After the predetermined reaction time, the reactor was rapidly cooled down to room temperature and the residual gases were discharged. The reaction mixtures containing liquid and solid fractions were centrifuged at 3000 rpm for 15 min and then vacuum-filtered to obtain a clear solution.

HPLC analysis of the product mixture from hydrothermal reaction

The aqueous phase containing various water-soluble reaction products from hydrothermal liquefaction of DSB was analyzed using a Jasco chromatographic separation module consisting of a model PU-2089 quaternary low pressure gradient pump, a model RI-2031 refractive index detector and a model LC-NetII/ADC hardware interface system. All solution samples were filtered through a 0.22 μm PVDF syringe filter prior to injection in the HPLC. The analysis of monomeric sugars including glucose, fructose, xylose, galactose and arabinose was conducted with an Aminex HPX-87P sugar column (Bio-Rad, 300 × 7.8 mm) using degassed HPLC-grade water isocratically flowing at a rate of 0.60 ml min^{-1}. The column was operated at 358.2 K and detection of effluent sugars was performed by using a RI-2031 detector. For the analysis of simple organic acids (*i.e.*, formic, acetic and levulinic acids) and furan derivatives (*i.e.*, 5-HMF and furfural), the separation of compounds was achieved with a Bio-Rad Aminex HPX-87H column (300 × 7.8 mm) using isocratic elution of sulfuric acid aqueous solution (5 mM) as the mobile phase at a flow rate of 0.60 ml min^{-1}. The RI-2031 detector was used to identify the compounds and the column oven was set to 328.2 K. The concentrations of each compound in the product mixture were determined using the calibration curves obtained from the injection of solutions of authentic samples with known concentrations.

Gas chromatography analysis of the reaction products containing GVL

The reaction products containing GVL were quantitatively analyzed by using a Shimadzu GC-2014 gas chromatograph equipped with a Phenomenex Zebron™ ZB-Wax capillary column (30 m length × 0.32 mm i.d., 0.25 μm film thickness) and a flame ionization detector (FID). The carrier gas was ultra-high purity (UHP) grade helium (99.99%) with a constant flow rate of 1.0 ml min^{-1}. The injection volume was 1.0 μl in splitless mode. The following temperature program was used in the analysis: an isothermal step at 60 °C (held for 3 min), which was ramped at a rate of 10 °C min^{-1} to 230 °C and held for 5 min. The injector and detector temperatures were kept at 250 and 300 °C, respectively. The identification of reaction products was accomplished by comparison of sample peak retention times with those of authentic standards analyzed under identical conditions. Standard solutions encompassing the

concentration range of the samples were used to construct the calibration curves for quantifying the concentrations of the compounds of interest.

Results and discussion

The characteristics of SB and DSB samples include elemental and proximate compositions and their lignocellulose contents are presented in Table 1. In order to examine the thermal stability of biomass precursor, TGA was conducted under nitrogen environment by raising the temperature gradually from ambient to an upper limit of 1073.2 K, where it is safely assumed that all the elemental oxygen and hydrogen are liberated to gaseous compounds, thus leaving only elemental carbon. TGA result indicates that SB is a potential feedstock for energy and chemical production due to high cellulose (35.4%) and hemicellulose (24.7%) contents, which are the main sources of fermentable sugars. From TGA curves shown in Fig. 1, it is clearly seen that SB sample undergoes a gradual thermal decomposition process with a significant weight loss happening at temperatures between 260 and 360 °C. The weight loss of about 60% corresponds to the rapid breakdown of hemicellulose and cellulose fractions with the DTG peak temperatures at 295 and 352 °C, respectively. The degradation of lignin might also happen over this temperature range, which is primarily caused by the breakdown of chemical bonds with low activation energy.[31] A minor weight loss about 5% occurring between 400 and 500 °C is attributed to the lignin degradation reaction involving the breakdown of more stable bonds. The temperature regions where depolymerization of hemicellulose and the random cleavage of the glycosidic linkages in cellulose structure occur are in good agreement with the studies of Yang *et al.*,[31] Garcia-Perez *et al.*[32] and Cao and Aita.[33] At high temperatures between 500 and 800 °C, the weight loss signal was not very evident, approaching a value for the charcoal yield of 15.7%. The cellulose, hemicellulose and lignin contents (on a dry basis) of SB sample obtained from TGA method are in good agreement with the values determined from "wood-industry" methods and the established protocols of National Renewable Energy Laboratory (NREL). The thermogravimetric curve of DSB sample shows a similar characteristic to that of SB sample with higher onset of degradation temperatures for hemicellulose and cellulose at 306 and 364 °C, respectively. This indicated that the treated biomass exhibited higher thermal stability due to the lignin and hemicellulose removal. Maximum rates of weight loss occur between 270 and 380 °C for delignified biomass. Again, the amount of weight loss was insignificant at high temperatures between 500 and 800 °C, yielding residual carbon of 17.2%. The individual monosaccharides include glucose, xylose, galactose and arabinose present in the hydrolysate solution obtained from dilute acid hydrolysis (5% HCl under reflux at 96 °C for 2 h) of SB and DSB samples were quantified with a chromatographic procedure of du Toit *et al.*[34] and the monomeric sugar yields, in the unit of mg g^{-1} dry biomass, were given as follows: glucose (387.4) for SB and (564.2) for DSB, xylose (245.5) for SB and (188.2) for DSB, galactose (2.8) for SB and (2.1) for DSB and arabinose (31.4) for SB and (22.8) for DSB. In this respect, the concentrations of the polymeric sugars corresponding to its monosaccharide units (Table 1) are calculated according to NREL conversion formula.

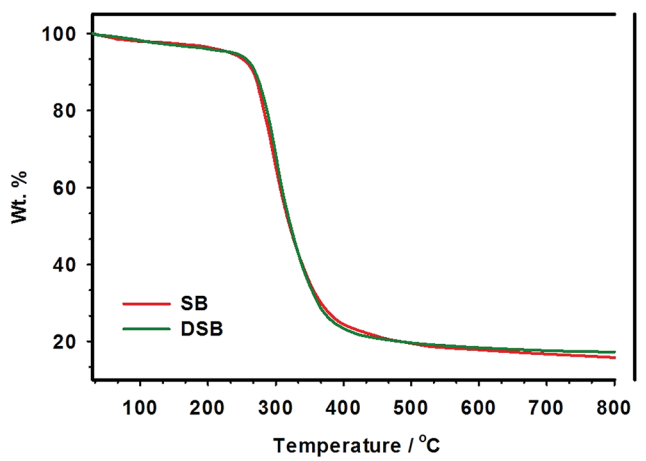

Fig. 1 Thermogravimetric curves of sugarcane bagasse before (SB) and after NaOH delignification pretreatment (DSB).

Lignin can act as a physical barrier, encapsulating and confining cellulose and this complex three-dimensional aromatic polymer architecture is highly recalcitrant toward enzymatic, chemical and biological degradation. Therefore, pretreatment strategy to promote efficient hydrolysis is an essential step in the lignocellulosic biomass-processing biorefineries to reduce the inherent lignocellulosic cell wall recalcitrance for cost-effective downstream processing. Since the biomass feedstock contains a quite high portion of lignin (21.8%), delignification pretreatment with NaOH solution is employed to effectively remove lignin from the biomass, at the expense of parts of the structural carbohydrates are decomposed. After delignification, the lignin content significantly decreased from 21.8% in the native biomass to 10.3% in the treated biomass. In line with this, the concentrations of polymeric hemicellulose sugars including xylan, galactan and arabinan in the treated biomass were 165.6, 1.9 and 20.2 mg g^{-1} dry biomass, respectively, indicating that alkaline delignification brought hemicellulose dissolution. On the other hand, most of the glucan portion was preserved during delignification pretreatment, which could be ascribed to the robust crystalline structure and low reactivity of cellulose with alkali. For comparison purposes, the alkaline delignification conditions of various lignocellulosic biomass resources are listed in Table 2. From this table, it can be shown that delignification efficiency varies greatly with process conditions and types of the biomass feedstocks. In general, alkali pretreatment is more effective for removing a substantial portion of lignin from hardwood biomass and agriculture waste products. Moreover, the delignification efficiency under conditions described in this study (52.8%) compares well with other studies performed at higher temperatures (*e.g.*, 368.2, 394.2 and 433.2 K) and shorter residence time (*e.g.*, 1, 1.5 and 3 h) in the absence of stirring. The main chemical mechanism by which the lignin polymer degrades in alkaline and alkaline-oxidative environments has

Table 2 Summary of alkaline delignification conditions of various lignocellulosic biomass resources

	Delignification conditions					
Lignocellulosic resources	Alkali	Solid–liquid ratio (w/v)	Temperature (K)	Residence time	Stirring speed (rpm)	Delignification efficiency (%)
Sugarcane bagasse – Aita *et al.*[33]	NH_4OH	1 : 20	433.2	1 h	NA	14
Corn stalk – Yu *et al.*[35]	NaOH	1 : 15	333.2	1.5 h	NA	60
Corn stover – Kim and Holtzapple[36a]	$Ca(OH)_2$	1 : 2	328.2	4 weeks	NA	87.5
Sorghum – Salvi *et al.*[37a]	NH_4OH	2 : 1	433.2	1 h	NA	44
Cotton stalk – Silverstein *et al.*[38]	NaOH	1 : 10	394.2	1.5 h	NA	65.6
Switchgrass – Gupta and Lee[39]	NaOH	1 : 10	358.2	24 h	NA	76.1
	NH_4OH	1 : 10	393.2	24 h	NA	67.8
Mixed hardwood chips – Yu *et al.*[40b]	GL	1 : 4	433.2	Not available	NA	28.8
Rice straw – Cheng *et al.*[41c]	NaOH	5 : 1	328.2	3 h	NA	23.1
	$Ca(OH)_2$	10 : 1	368.2	3 h	NA	24.4
Sugarcane bagasse – this study	NaOH	1 : 10	Room	24 h	500	52.8

[a] The loading ratios of alkali to raw biomass are given on a mass basis. [b] GL (green liquor) is an alkaline solution prepared by mixing sodium carbonate and sodium sulfide with a sulfidity of 25%. [c] The loading ratio is expressed as g H_2O g^{-1} oven-dried rice straw with an alkali loading of 4 wt% for NaOH and 10 wt% for $Ca(OH)_2$.

been mechanistically studied and is through the cleavage of hydrolysable α- and β-aryl ether bonds in lignin and glycosidic bonds in polysaccharides. Meanwhile, hemicellulose dissolution and cellulose swelling are a consequence of hydrogen bond weakening. The post-pretreatment biomass washing step by warm or hot distilled water aims to remove the alkali residues, soluble phenolics and other degradation products formed during lignin depolymerization. In this regard, the concentration of alkali metal ion remained with the washed biomass was very low or absent after repeated washing step. The pretreatment liquor from delignification step containing dissolved lignin, lignin-derived soluble phenolics, acetic acid, hemicellulose-derived poly/oligosaccharides, proteic compounds and other extractives can be reclaimed for further applications such as production of bioethanol or biohydrogen.

Alkaline delignification pretreatment had a notable effect on the biomass morphology. Images obtained by SEM show some visible changes associated with the biomass wall disruption after delignification. The rod-like morphology of native biomass (SB) was easily recognizable in Fig. 2(a) and the untreated SB had a relatively smooth and intact surface. Delignification pretreatment by NaOH resulted in the disrupted surface structure due to the breakdown of lignin as shown in Fig. 2(b) and therefore the surface of delignified biomass (DSB) appears rougher when compared to the native biomass. Moreover, the structure of DSB biomass was opened up as a result of lignin removal, indicating the more available or exposed surface area of cellulose for hydrolysis. Fig. 2(c) depicts the morphological features of DSB biomass wall after sub-CW treatment. The surface structure of sub-CW treated DSB biomass changed significantly when compared with DSB sample, showing a sponge-like structure. The small pores/cavities formed on the wall of sub-CW treated DSB sample might be the result of release of hemicellulose or cellulose decomposition products from the interior of the biomass particle. Fig. 2(d) shows the aggregates of irregularly-shaped, non-uniform solid particles obtained from hydrothermal conversion of DSB sample. The size distribution of the solid aggregates ranged from tens of microns to submicron. The electron micrograph clearly reveals that spherical particles were not likely formed in the hydrothermal processing at low temperatures. Titirici and group[42] obtained sphere-shaped and monodisperse hydrothermal carbons derived from pure glucose at 533.2 K while the overall morphology of hydrothermal carbons derived from cellulose and rye straw (a model of lignocellulosic biomass) was not as homogeneous as from pure glucose, with some structural components of the precursor material still remained intact and arranged together with spherical carbon particles. The elemental composition analysis was conducted by an INCA energy dispersive X-ray microanalysis system integrated with the hardware of the SEM and result showed that the solid

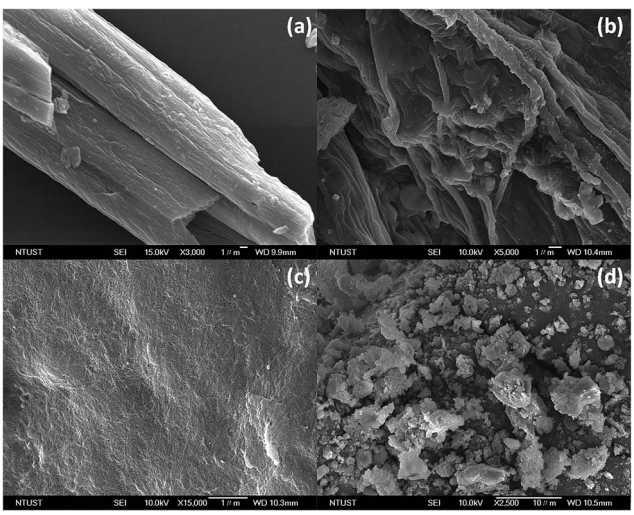

Fig. 2 Scanning electron micrographs of untreated sugarcane bagasse – SB (a) and after NaOH delignification pretreatment – DSB (b), morphological structure of biomass (DSB) wall following sub-CW treatment (c) and solid 'humin' byproduct obtained from hydrothermal conversion of DSB biomass (d).

aggregates were comprised of elemental carbon (64.8 at%) and oxygen (35.2 at%).

The morphological features of the catalysts are depicted in Fig. 3. From SEM images, it can be seen that UB catalyst is aluminosilicate clay with a layered structure and smooth surface. The specific surface area of UB catalyst calculated from the BET method was 61.8 $m^2\ g^{-1}$ and its total pore volume was $8.3 \times 10^{-2}\ cm^3\ g^{-1}$. Nitrogen adsorption–desorption isotherms revealed a classical combination of micro/mesoporous structures in the catalyst particle. After chemical modification by sulfuric acid, some evident changes in the platelet morphology of UB catalyst were observed. Generally speaking, an acid treatment results in the replacement of exchangeable cations that are between the layers (*i.e.*, Na^+, K^+ or Ca^{2+}) with H^+ ions of the acid and depending on the treatment conditions, partial delamination of Al-octahedral and Si-tetrahedral layers, followed by subsequent dissolution of structural cations (typical examples are $Fe^{2+/3+}$, Mg^{2+} or Al^{3+} in the Al-octahedral layer and Al^{3+} or Si^{4+} in the Si-tetrahedral layer).[43] The small difference in CEC between UB (58.3) and AAB (57.5) samples suggests that the structural cations in the Al-octahedral and Si-tetrahedral layers are marginally affected by dilute acid attack. The surface acidity (or catalytic acid sites) of the bentonite, as determined by a simple acid–base titration method,[44] increased dramatically from 30.7 (UB) to 118.2 meq. 100 g^{-1} clay after treatment by 2 N sulfuric acid. Results of nitrogen adsorption–desorption measurements for AAB catalyst show an increase in the BET specific surface area and total pore volume. The BET specific surface area and total pore volume of AAB catalyst are 122.4 $m^2\ g^{-1}$ and 0.12 $cm^3\ g^{-1}$, which is ~2- and ~1.5-fold higher compared to those values of UB catalyst. The scanning electron micrograph of 1% Pt@TiO_2 in Fig. 3(b) shows that the catalyst is spherical-like irregular particles with average diameter sizes are in the submicrometer range (150–200 nm). The BET specific surface area of 1% Pt@TiO_2 was lower compared to bare TiO_2 (48.4 *vs.* 51.3 $m^2\ g^{-1}$), likely due to the deposition of fine Pt particles on the surface of the support that might block pores of TiO_2.

The wide angle XRD patterns of AAB and 1% Pt@TiO_2 catalysts are shown in Fig. 4. From the XRD spectrum of AAB catalyst, the montmorillonite (2θ = 6.7°, 20.2°, 21.8°, 35.1° and 61.8°) and quartz (2θ = 26.8°, 50.4° and 68.3°) are the major phases with other minor reflections corresponding to mineral impurities of crystobalite, calcite, K-feldspar, mica and/or illite phases. The reflection at 2θ = 6.7° is correlated to the basal spacing (001) of montmorillonite, corresponding to a value of 1.32 nm. Compared to UB catalyst, the position of the (001) basal reflection in AAB catalyst remains essentially unchanged (2θ = 6.8°, 1.30 nm), showing the minor effect of dilute acid treatment on the lattice structure of clay. As it can be seen from Fig. 4(b), the bare TiO_2 exhibits reflections at 2θ angles of 25.5°, 37.2°, 38.0°, 48.1°, 54.4°, 55.2°, 62.7° and 68.9° in which all these reflection peaks can be well indexed to the (101), (103), (004), (200), (105), (211), (204) and (116) crystal planes of TiO_2 with anatase phase according to JCPDS database card no. 21-1272. The diffraction lines for (111), (200) and (220) of Pt cubic phases were located at about 2θ angles of 39.8°, 46.4° and 67.5° (JCPDS database card no. 04-0802). Result showed that the diffraction pattern of 1% Pt@TiO_2 was essentially the same as that of diffraction pattern from bare anatase TiO_2. Similar observations have been noted by Zhang *et al.*[30] and Moonsiri *et al.*[45] in their studies. The absence of diffraction signals from metallic Pt species could be attributed to the small size and highly distributed Pt particles supported on TiO_2. Zhang and co-workers[30] observed that Pt particles were highly dispersed on TiO_2 support into a size smaller than 1 nm from high-resolution transmission electron microscope (HRTEM) image. Hence, we believe that in case of fresh 1% Pt@TiO_2 catalyst, the average Pt particle sizes are around 1 nm (or even smaller) since the catalyst preparation in our study was adopted from Zhang *et al.* procedure. The high dispersion of nano-sized Pt particles on anatase TiO_2 support could be very important for high activity and selectivity of this catalyst in the hydrogenation of LA.

In the hydrothermal reaction with the aim of producing building block chemicals for clean liquid fuels, the cellulose and hemicellulose components of biomass were hydrolyzed to six and five carbon sugar monomers, followed by dehydration reactions of these monomeric sugars to produce 5-HMF and furfural in water under subcritical condition. Given the fact that sub-CW possesses the catalytic role of an acid or base and has been widely used as an alternative medium for the conversion of lignocellulosic biomass into platform chemicals, Table 3 presents the conversion yields of cellulose and hemicellulose components of DSB biomass into a variety of reaction products including sugars, 5-HMF, furfural and organic acids in the absence or presence of solid acid catalysts. From this table, it is easily noticed that the performance of non-catalyzed, mildly sub-CW treatment for cellulose hydrolysis is not so impressive with glucose yield ranged between 32.74 and 54.18 mg g^{-1} dry biomass (3.27–5.42 wt%) in the temperature range of 393.2–473.2 K for 60 min reaction. The incomplete and slow conversion rate of cellulose into glucose under non-catalyzed, mildly sub-CW treatment might be due to the fact that hydrolysis reaction was limited at the surface region without cellulose swelling and dissolution compared to the reaction taking place in high-density regions (near-critical and supercritical water)[46] as well as insufficiently high temperature to disrupt the robust structure of cellulose. Hemicellulose-derived monosaccharides were also present in the reaction product mixture, accounting for 3.3–4.1 wt% yields. The quantities of 5-HMF and LA were barely detectable in the reaction product mixture, affording

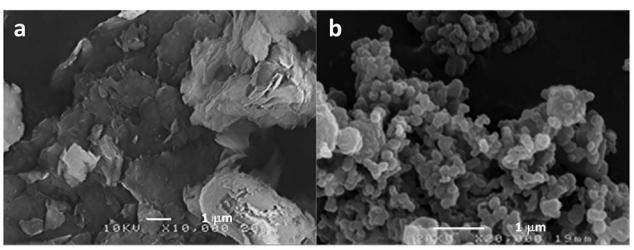

Fig. 3 Scanning electron micrographs of AAB clay (a) and 1% Pt@TiO_2 catalysts (b).

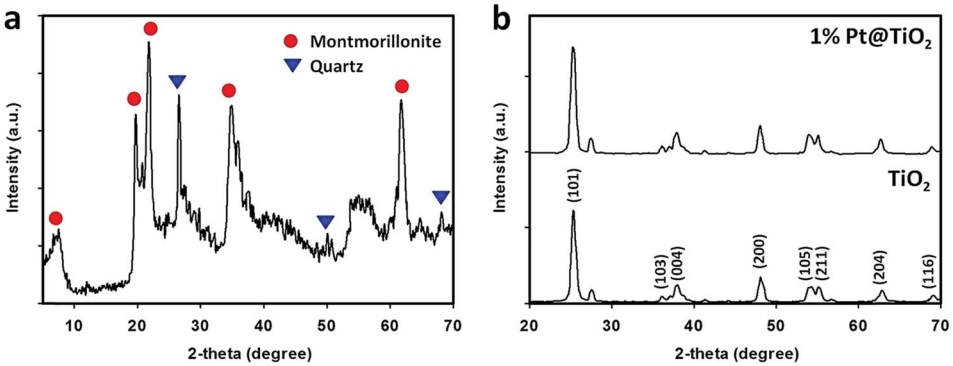

Fig. 4 XRD patterns of AAB (a) and bare TiO_2 and 1% Pt@TiO_2 catalysts (b).

Table 3 Non-catalytic and catalytic results of sub-CW treatment of DSB biomass in the presence of 2% (w/v) UB or AAB clay-based catalysts at various temperatures for reaction time of 60 min

		Yields (mg g^{-1} dry biomass)								
Sub-CW treatments	T (K)	Glucose	Xylose	Arabinose	Galactose	5-HMF	LA[a]	FA[a]	Furfural	AA[a]
Non-catalytic	393.2	32.74	28.36	4.24	0.28	0.76	0.08	0.01	0.52	0.58
	413.2	35.56	29.70	4.44	0.30	0.90	0.11	0.02	0.61	0.71
	433.2	42.33	32.41	4.83	0.32	1.16	0.16	0.04	0.74	0.87
	453.2	54.18	35.69	5.33	0.35	1.67	0.28	0.09	0.95	1.02
	473.2	50.69	33.25	5.02	0.37	1.49	0.23	0.12	0.88	1.14
UB-catalyzed	393.2	38.38	41.47	6.20	0.42	2.18	0.44	0.14	5.49	0.80
	413.2	46.28	43.01	6.43	0.44	2.82	0.65	0.23	6.64	0.93
	433.2	54.19	47.45	7.09	0.49	3.60	0.89	0.34	8.03	1.09
	453.2	89.41	63.08	9.42	0.67	6.79	3.14	1.38	14.38	1.17
	473.2	78.56	54.25	8.18	0.63	5.54	2.76	1.59	13.15	1.32
AAB-catalyzed	393.2	92.00	58.64	8.76	0.62	23.18	30.52	9.10	28.90	1.41
	413.2	115.71	64.82	9.68	0.67	30.78	43.64	14.30	32.90	1.64
	433.2	145.06	72.33	10.81	0.75	41.63	74.78	23.68	37.78	1.90
	453.2	216.75	95.30	14.35	0.93	80.41	159.17	55.09	53.87	2.23
	473.2	190.46	86.71	12.62	0.91	65.69	125.44	61.72	46.48	2.56

[a] LA, FA and AA represent levulinic acid, formic acid and acetic acid, respectively.

yield less than 0.2 wt%. In pure sub-CW medium, the dehydration of glucose into 5-HMF is non-selective,[47] leading to formation of multiple side-products and insoluble carbonaceous residue 'humin'. The reaction mixture after sub-CW treatment also turned into dark brown, which could be ascribed to the formation of soluble and insoluble polymeric side-products. These polymeric side-products were not characterized in this study due to several analytical issues. The presence of furfural was detected in the reaction product mixture and a maximum yield of 0.95 mg g^{-1} was achieved at 453.2 K. The furfural yield for non-catalyzed, mildly sub-CW treatment in this study compares well with results in the literature for a one-stage process where hydrolysis and dehydration reactions occur simultaneously within the same reactor.

In the absence of catalysis, the hydrothermal degradation rate of cellulose to glucose is not significant. It was later revealed by Kuster[48] that the enolization rate of glucose, a rate-determining step for 5-HMF formation, is slow in water and intermediate 5-HMF is more likely to undergo a series of unwanted side reactions such as condensation, rehydration, fragmentation and cross-polymerization reactions involving sugars, water molecules and various reactive intermediates. The use of heterogeneous solid acid catalysts for enhanced cellulose conversion and also selective and high-yielding production of 5-HMF and LA has been coming up to a promising direction of research. In this regard, clays and clay minerals can catalyze chemical reactions *via* Bronsted and/or Lewis acid sites on their surfaces although native or natural clays generally show low or almost no catalytic activity prior to acid or cation exchange treatments. As expected, the cellulose conversion catalyzed with UB solid slightly enhanced compared with blank reaction (no catalyst) and the glucose yield reached only 89.41 mg g^{-1} dry biomass for 60 min reaction at 453.2 K. Low catalytic activity of untreated bentonite might lead to speculation that the solid acid catalyst is not active enough for promoting hydrolysis of cellulose, possibly attributed to: (1) the surface of solid acid catalyst cannot readily adsorb or attach to cellulose and β-1,4 glucan in water or (2) the absence of freely available, strong Bronsted acid sites for decomposing hydrogen bonds and hydrolyzing β-1,4 glycosidic bonds in cellulose. Under the same

reaction condition, 5-HMF and LA with the corresponding yields of 6.79 and 3.14 mg g^{-1} dry biomass were produced. Based on the results obtained, it could be inferred that the product distribution was affected by addition of UB catalyst while minor improvement on the cellulose conversion in water was observed compared to blank reaction. Moreover, the yield values of 5-HMF and LA are higher than those obtained from blank reaction, showing that water, in the presence of acid catalyst, is a favorable medium for promoting rehydration of 5-HMF to LA. Very recently, Li and his team[49] demonstrated that the decomposition of 5-HMF to LA was the preferred reaction pathway in water and an unexpectedly high LA yield could be obtained in the presence of Amberlyst™ 70 as the solid acid catalyst. Under our experimental conditions, fructose was present at trace level in the reaction product mixture either due to limited extent of glucose isomerization to fructose or once formed, fructose was rapidly dehydrated to 5-HMF.[50] The temperature variation experiments for UB-catalyzed hydrothermal treatment showed an upward trend of cellulose depolymerization rate with temperature. The actual yields of glucose, 5-HMF and LA increased when the reaction temperature was raised from 393.2 to 453.2 K and a decrease in yield was noted at 473.2 K. Such results imply that an increase in temperature not only improves the extent of cellulose depolymerization, but also enhances the rate of side reactions.

The actual yields of pentoses increased to the range of 47.67–72.50 mg g^{-1} dry biomass, indicating that UB catalyst was active for hemicellulose conversion. Over the temperature range studied, *ca.* 0.55–1.44 wt% furfural yields were achieved with UB catalyst having a Si/Al molar ratio of 5.3. A similar increasing trend in pentoses and furfural yields from hemicellulose conversion over synthetic zeolites (HBeta, HMOR and HUSY) and K10 montmorillonite catalysts has been demonstrated as well.[51] The increase in furfural yield implies that the Bronsted acid sites located at the external surface of the Si-tetrahedral layer (one may refer to the terminal silanol groups, $Si–OH_2^+$) are particularly active in catalyzing the dehydration of xylose to furfural. The effects of catalyst loading on the yields of sugars, 5-HMF, furfural and LA were investigated by varying the catalyst amounts from 0 to 2% (w/v) for 60 min reaction at 473.2 K. Experimental results depicted in Fig. 5 show that higher yields of LA and furfural could be obtained by increasing the catalyst loading from 1 to 2%, due to a higher number of catalytic acid sites are available for reaction. Further increase in the catalyst loading may or may not adversely affect the formation of LA and furfural and optimization of the catalyst loading is beyond the scope of this study.

Table 4 summarizes comparison of hexoses (*e.g.*, glucose and fructose), xylose and other carbonaceous feedstocks (cellulose and hemicellulose) conversion into 5-HMF, LA and furfural over solid acid catalysts having only Bronsted acid sites or rationally designed by varying the Bronsted-to-Lewis ([B]/[L]) acid site ratios such as H-mordenite, ion-exchange polymeric resins (Amberlyst™ 15 and Amberlyst™ 70), Sn-exchanged montmorillonite, acid-functionalized mesoporous SBA-15, K10 montmorillonite and metal oxides catalysts (TiO_2 and ZrO_2). In this table, it can be seen that most studies used commercial sources

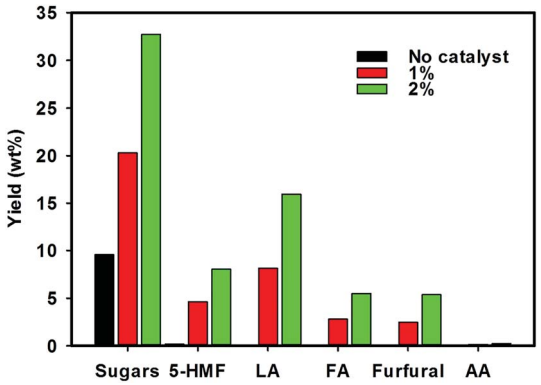

Fig. 5 Effect of AAB solid acid catalyst load amounts on the yields of reaction products obtained from hydrothermal conversion of DSB biomass at 453.2 K.

of high purity sugars or microcrystalline cellulose (MCC, Avicel®) as model compounds to produce 5-HMF or furfural as end products. For this case, the product selectivity term is defined as the mol% yield of targeted product divided by mol% of reactant consumed or mathematically described by: selectivity, S (%) = product yield (mol%)/conv. (mol%). Using simple carbon sources such as glucose, xylose or other mono/disaccharides, it is reasonable to achieve moderate to very high selectivity toward targeted product due to simpler and better control in reaction within one reactor. Following this statement, the determination of product selectivity term by the above mathematical expression for direct conversion pathways such as from glucose or fructose into 5-HMF, from MCC into LA or from xylose or hemicellulose into furfural is deemed to be valid. On the other hand, there still exists conflicting definitions for the product yield and selectivity terms in the study utilizing real lignocellulosic biomass. In such typical cases, the conversion of lignocellulosic biomass into platform chemicals involves a complex multi-step route. Another potential issue to consider is the determination of initial amount (moles) of biomass reactant fed into the reactor may not be possible unless a thorough characterization study (*e.g.*, gel permeation chromatography or cross-polarization magic angle spinning ^{13}C-NMR spectroscopy) is performed to interpret the molecular mass of biomass. Thus, the product selectivity term for hydrothermal conversion step is not evaluated in this paper due to a set of main and side reactions are involved during the indirect conversion of DSB biomass to LA and several reaction products remained unidentified by HPLC analysis, which may overestimate true selectivity values. Another reason was due to the instrumentation issues for conducting a thorough characterization of biomass feedstock in this study.

On the contrary, the cellulose conversion to glucose and rehydration of 5-HMF to LA was quite significant with AAB as a solid acid catalyst (Si/Al molar ratio = 6.8). AAB catalyst also possesses dual Bronsted and Lewis acidity similar to the untreated bentonite; however the number of Bronsted acid sites appears to be higher than the Lewis acid sites after H_2SO_4 treatment. In this regard, the presence of Bronsted acid sites

Table 4 Conversion and selectivity in the aqueous-phase dehydration reaction of hexoses, xylose and other carbonaceous sources into 5-HMF, LA and furfural catalyzed by various solid acid catalysts

Entry	Catalyst	Reaction pathway	Selectivity (%)			Conv. (%)	Reference
			5-HMF	LA	Furfural		
1	LZY zeolite	Fructose → LA	6.5	84.4	—	96.0	50
2	HUSY zeolite	Hemicellulose → furfural	—	—	45.7	36.1	51
3	K10 montmorillonite	Hemicellulose → furfural	—	—	67.0	24.6	51
4	H-mordenite (Si/Al = 11)	Fructose → 5-HMF[a]	91.0	—	—	76.0	52
5	HY zeolite	Xylose → furfural	—	—	22.7	62.3	53
6	Sn-beta/HCl zeolite	Glucose → 5-HMF	6/72[a]	—	—	45/79[a]	54
7	Amberlyst™ 15	Glucose → 5-HMF[a]	8.9	—	—	78.7	55
8	Sn-exchanged montmorillonite	Glucose → 5-HMF	16.2/54.4[a]	—	—	40.2/98.4[a]	55
9	Ca-montmorillonite	Glucose → 5-HMF[a]	0	—	—	48.0	55
10	Amberlyst™ 70	Xylose → furfural	—	—	99.8	8.0	53
		Fructose → 5-HMF[a]	60.0	—	—	85.0	56
11	Acid-functionalized SBA-15	Fructose → 5-HMF[a]	66.0	—	—	79.0	56
12	Anatase TiO_2	Glucose → 5-HMF	16.5	—	1.2	85.0	57
13	Zirconia	Fructose → 5-HMF	15.6	—	1.1	90.0	57
14	Zirconia	Cellulose → LA	2	53.9	8.0	100	58
15	Tungstated alumina (AlW)	Cellulose → LA	—	6.4	—	47	59

[a] Dehydration reactions were carried out in biphasic systems such as in water/methyl isobutyl ketone (Entry 4), H_2O/THF with 0.35 g salt per g H_2O (Entry 6), THF/DMSO (Entries 7–9), aqueous and methyl isobutyl ketone/2-butanol phases (Entry 10: fructose → 5-HMF, Entry 11).

located at the external surface of the Si-tetrahedral layer and in the interlayer region can serve as the catalytic acid sites for hydrolysis of cellulose to glucose and rehydration of 5-HMF to LA. The Bronsted acid sites in the acid-activated clay might also coordinate with hydroxyl groups bonded with Al^{3+} cations in the Al-octahedral layer based on FTIR spectroscopic study of Tyagi and his group.[60] The selective hydrolysis of cellulose to glucose over various solid acid catalysts include a robust sulfonated activated carbon (AC-SO_3H) catalyst at 423.2 K has been conducted by Onda and co-workers.[44] Further, they found that the AC-SO_3H catalyst displayed significant catalytic activity and a remarkably high selectivity toward glucose production, which was attributed to high hydrothermal stability, strong acidic SO_3H groups and the hydrophobic graphene planes of the catalyst. Tong and co-workers[61] conducted catalytic hydrolysis of cellulose to reducing sugar in water over acid-activated montmorillonite catalysts and their study showed that the higher concentrations of the Bronsted acid sites in the interlayer region contributed to greater conversion of cellulose. Since AAB possesses a micro-mesoporous structure with slit-shaped pores of 3–4 nm in diameter, it can be argued that the internal diffusion limitation may not be significant. The molecular dimensions of monomeric sugars and their degradation products are found to be similar to pore sizes of microporous materials (0.4–0.9 nm),[62] thus the 3 to 4 nm-sized pores are large enough for monomeric sugars, furans (5-HMF and furfural) and simple organic acids (LA) to diffuse in and out of the catalyst particle. Once monomeric sugars or intermediate oligomers (*e.g.*, dimers, trimers or tetramers) are formed within pores, these molecules can enter narrow channels in the catalyst particles and interact with internal acid sites to give furans and LA. The Lewis acidity associated with the clay edge sites, although less prominent than the Bronsted acid sites, might also take part in the catalytic reaction. The Lewis acid sites on clays can also be generated due to octet vacancies that occur as a result of structural metal cations (*e.g.*, Mg^{2+} or Al^{3+}) being carried away during acid activation. However, the extent of catalysis by the Lewis acid sites toward the rates of cellulose and hemicellulose depolymerization remains unknown in our experiments. The polymerization reactions leading to formation of soluble and insoluble polymeric side-products did occur in the sub-CW treatment catalyzed by AAB solid, but to a lesser extent compared to blank and UB-catalyzed sub-CW treatments. It is anticipated that the catalyst mesoporosity might enhance diffusion of furan and LA products away from the active sites where hydronium-catalyzed side and secondary reactions could occur. In consequence, higher LA yield was obtained in the AAB-catalyzed sub-CW treatment as shown in Table 3. The yield of LA ranged between 30.52 and 159.17 mg g^{-1} dry biomass in the AAB-catalyzed sub-CW treatment, representing a significant increase in yield over the range of values obtained from UB-catalyzed sub-CW treatment. Therefore, an aqueous solution containing LA (15.92 wt%) obtained from AAB-catalyzed sub-CW treatment at 453.2 K and 2% catalyst loading was further used in the catalytic hydrogenation process to produce GVL.

Saturated lactone (GVL) can be synthesized from an aqueous solution containing LA by catalytic hydrogenation reaction. For this reaction, it is well recognized that supported catalysts featuring noble metals such as platinum and ruthenium in nano-sizes and highly dispersed form are the most active and product selective toward GVL. In the catalytic hydrogenation of LA to GVL, the reaction pathways can be distinguished into two main routes, depending on the order in which dehydration and hydrogenation occur:[63] (i) acid-catalyzed dehydration of LA into angelica lactones (ALs, α or β isomers) as intermediate followed by hydrogenation of ALs to GVL (*i.e.*, dehydration–

hydrogenation route) or (ii) direct synthesis through 4-hydroxypentanoic acid (4-HPA) which subsequently undergoes highly favorable acid-catalyzed intramolecular esterification (ring closure) to five member ring GVL (*i.e.*, hydrogenation–dehydration route). Results for the effects of reaction time and temperature on the conversion and GVL selectivity in Pt@TiO_2-catalyzed hydrogenation of LA are shown in Table 5. In this table, it can be seen that the conversion of LA increased with the extension of reaction time, from 59.3% (120 min) to 88.5% (360 min) at 433.2 K. The same promoting effect was noticed for temperature, in which higher LA conversion was achieved by conducting the reaction at higher temperatures. The best catalytic activity shown by 1% Pt@TiO_2 catalyst was observed at 473.2 K for 360 min reaction, corresponding to 99.3% GVL yield (99.3% selectivity at 100% conversion). The selectivity of 1% Pt@TiO_2 catalyst toward GVL in this work was considerably higher than that reported by Upare and co-workers[64] for 5% Pt@C catalyst (30% selectivity at 100% conversion). The difference in hydrogenation activity between Pt@C and Pt@TiO_2 catalysts might be attributed to the nature of the support material in which TiO_2 support could adsorb and activate the carbonyl group of LA and consequently enhance the catalytic activity several times with respect to conventional Pt supported on carbon that does not perform such activation.[65] Another explanation proposed in the literature for high GVL selectivity over titania-supported catalysts is the absence of strong acid sites that are responsible for formation of GVL decomposition products, for example, 2-methyl tetrahydrofuran (2-MTHF), valeric acid (VA) or 1,4-pentanediol (PD).[66] An excellent performance of 1% Pt@TiO_2 catalyst in the hydrogenation of LA was noticed in the study of Lange and his group,[67] yielding >90% conversion and >95% GVL selectivity for reaction at 473.2 K. A more recent study conducted by Ruppert *et al.*[66] also showed high GVL selectivity (81.8–97.6 mol%, 343.2 K) for the hydrogenation of LA in water over anatase or anatase/rutile mixed-phase TiO_2-supported platinum catalysts. Under our reaction conditions, the resulting byproducts from Pt@TiO_2-catalyzed hydrogenation of LA were 2-MTHF and VA, both formed with 0.6 and 4.2% selectivity at the upper and lower temperature limits for 360 min reaction. ALs was untraceable in the reaction product mixture, suggesting that this species was rapidly transformed into GVL under H_2 atmosphere and Pt@TiO_2 catalyst. Due to the fact that GVL is the dominant product, it seems that the role of TiO_2 support in the reaction pathway is limited to its interaction with platinum metal (adhesion and dispersion properties) and influencing the hydrogenation active sites on its surface. In order to investigate the role of AAB as a heterogeneous acid co-catalyst, the catalytic performance between 1% Pt@TiO_2 and 1% Pt@TiO_2 combined with AAB co-catalyst was compared in terms of conversion and GVL selectivity. When it comes to the selectivity, in the case of 1% Pt@TiO_2 catalyst, the primary product was GVL with >90% selectivity. Fig. 6 shows the compositions of reaction products obtained from catalytic hydrogenation of LA with 1% Pt@TiO_2 in combination with AAB co-catalyst. The results reveal that a similar product distribution consisting mainly of GVL (>92% selectivity) was obtained and only very few amounts of byproducts such as 2-MTHF and VA were detected. Full conversion of LA could be achieved at 413.2 K after 240 min reaction by utilizing combined catalyst system. Hence, AAB was demonstrated to be an effective acid co-catalyst, which contributed a remarkable positive effect on the catalytic performance. A similar finding has been reported by the group of Galletti *et al.*[68] for commercial ruthenium supported catalysts in combination with different heterogeneous acid co-catalysts include Amberlyst resins and niobium phosphate or oxide. Further studies on the rational design and optimization of the acid co-catalyst dosage and reaction tests under industrial viable conditions are still being carried out by our research group (Table 6).

Table 5 Effects of reaction time and temperature on the conversion and product yields in the catalytic hydrogenation of LA with 1% Pt@TiO_2 catalyst

			Yield (%)				
T (K)	Time (h)	Conv. (%)	GVL	AL	2-MTHF	VA	Selectivity[a]
393.2	2	35.3	32.0	—	1.6	1.7	90.7
	4	42.8	39.9	—	1.4	1.5	93.2
	6	54.4	52.1	—	1.0	1.3	95.8
413.2	2	47.1	43.5	—	1.6	1.9	92.4
	4	58.6	55.3	—	1.5	1.8	94.4
	6	72.2	69.7	—	1.1	1.4	96.5
433.2	2	59.3	55.9	—	1.5	1.8	94.3
	4	71.7	68.7	—	1.4	1.6	95.8
	6	88.5	85.9	—	1.2	1.4	97.1
453.2	2	77.8	74.3	—	1.7	1.8	95.5
	4	97.4	94.7	—	1.2	1.4	97.2
	6	100.0	98.4	—	0.7	0.9	98.4
473.2	2	93.6	90.8	—	1.3	1.5	97.0
	4	100.0	98.2	—	0.7	1.1	98.2
	6	100.0	99.3	—	0.2	0.4	99.3

[a] Selectivity was defined as the product yield (mol%) divided by LA conversion (mol%).

The catalyst stability and its possible reuse are both crucial issues with respect to economic and green chemistry considerations. Moreover, catalyst reuse considerably reduces both production costs and chemical waste, which is another critical issue of sustainability and environmental impact. The combined 1% Pt@TiO_2 and AAB co-catalyst was recovered from the decanted reaction mixture and reused five times. In detail procedure, a fresh charge of reactant was introduced into the reactor containing spent catalyst from the first reaction test and the subsequent catalytic run was continued. The recyclability results of the spent catalyst are shown in Fig. 7. It is clearly shown that there is a gradual decrease in the catalytic activity (conversion) and GVL selectivity after five consecutive catalytic runs, reaching a value of 87.4% conversion and 86.3% selectivity. This indicates that deactivation of the catalyst occurs during the subsequent reaction cycles, presumably due to coke formation from the polymerization of ALs over acidic AAB co-catalyst surface. The coke formation renders the catalyst less active, due to a decrease in the number of active surface sites available for hydrogenation. We also examined the extent of Pt metal leaching by performing inductively coupled plasma-mass

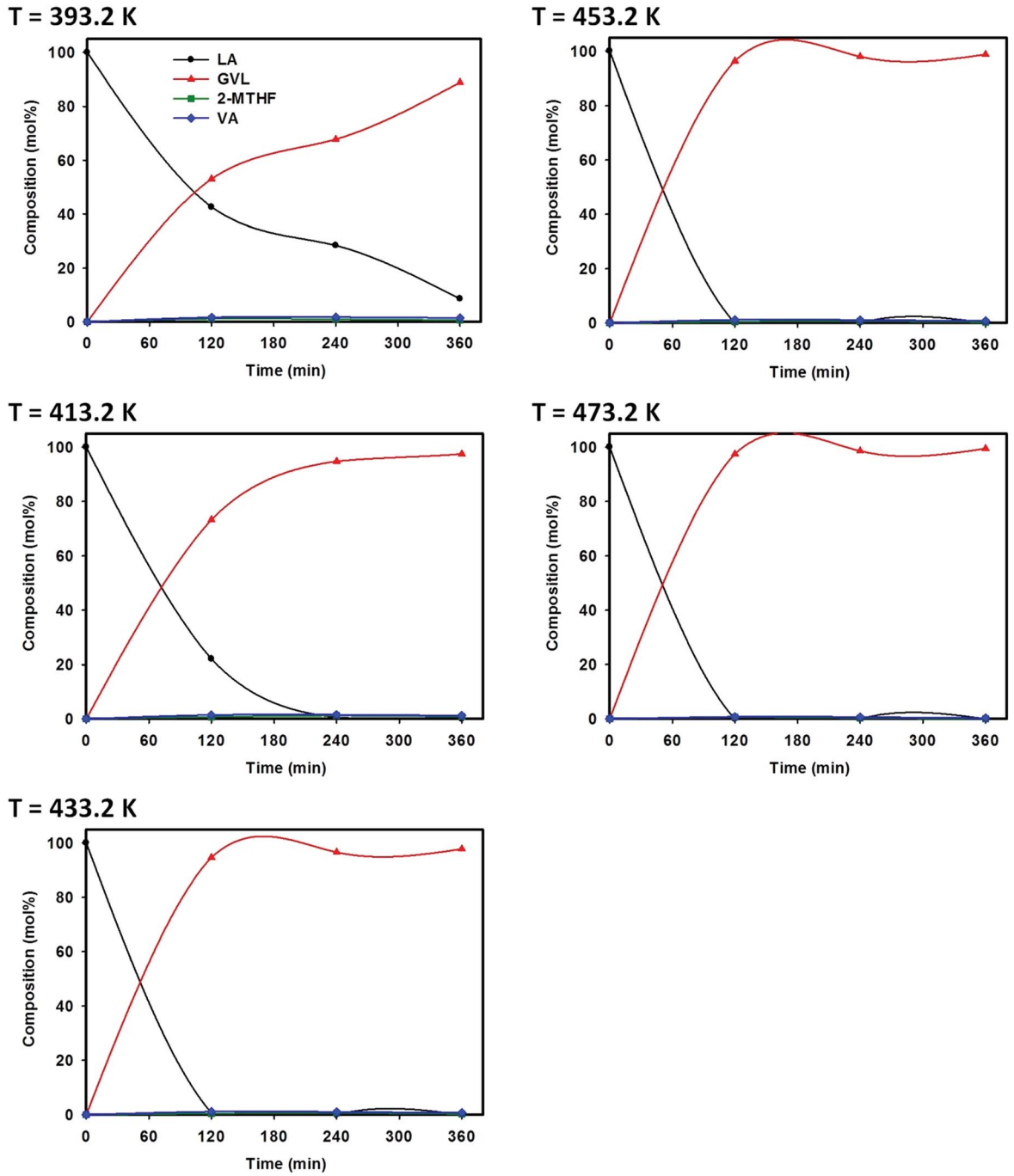

Fig. 6 Time and temperature effects on the hydrogenation of LA to GVL in the presence of 1% Pt@TiO_2 (0.25 g) and AAB clay (0.25 g) as an acid co-catalyst (LA: levulinic acid; GVL: gamma-valerolactone; 2-MTHF: 2-methyl tetrahydrofuran; VA: valeric acid).

spectrometry (ICP-MS) analysis in the liquid phase after 240 min reaction. The loss of the metal phase to the liquid phase was found to be very limited under applied reaction conditions. Hence, lower catalytic activity (LA conversion) and selectivity to GVL in the consecutive catalytic hydrogenation cycles points at deactivation of the spent catalyst by coking. In this regard, the spent catalyst after the fifth catalytic run was subjected to calcination at 723.2 K under a stream of pure oxygen for 180 min in order to remove as much carbon residue deposited on the catalyst surface as possible. By performing calcination at this temperature, the phase transformation of TiO_2 support, for example from anatase to rutile phase and the sintering or collapse of the 2 : 1 layer lattice structure of AAB clay do not occur and this appears to result in comparable catalytic performance of the calcined sample to that of fresh catalyst. The severe deformation of the layer lattice structures of clays and clay minerals was observed upon calcination at high temperatures (*i.e.*, 973.2–1473.2 K).[70]

Table 6 Comparison of the performance of various heterogeneous solid catalysts with or without co-catalysts in the hydrogenation of LA to GVL

	Hydrogenation Catalyst						
Entry	Metal	Particle size[a] (nm)	Support	Acid Co-catalyst	Conv. (%)	Selectivity to GVL (%)	Reference
Without acid co-catalyst							
1	Ru (5%)	2–5	Carbon	—	100	98.6	64
	Pd (5%)	17–18	Carbon	—	100	90	
	Pt (5%)	9	Carbon	—	100	30	
2	Ru (0.6%)	2	A-TiO_2[b]	—	100	93	65
3	Pt (1%)	4.5	A-TiO_2	—	54	92.6	66
		3.2	R-TiO_2[b]	—	27	85.2	
	Ru (1%)	—	A-TiO_2	—	38	81.6	
		2.2	R-TiO_2	—	95	87.4	
4	Pt (1%)	NA	A-TiO_2	—	>90	>95	67
5	Cu–Cr	NA	—	—	100	90.8	8
6	Ru (5%)	NA	Carbon	—	92	99	69
	Raney Ni	NA	—	—	19	32	
7	Cu	10–14	Zirconia	—	100	100	17
8	Pt (1%)	~1	A-TiO_2	—	58.6	94.4	This study
With acid co-catalyst							
9	Ru (5%)	NA	Al_2O_3	Niobium oxide	32	97.5	68
				Niobium phosphate	36	97.8	
				Amberlyst™ 70	57	98.6	
10	Pt (1%)	~1	A-TiO_2	Acid-activated bentonite	100	99.2	This study

[a] The metal particle sizes dispersed on the support materials were determined by using TEM/HRTEM, H_2 chemisorption or XRD techniques (NA = not available). [b] A-TiO_2: anatase TiO_2 and R-TiO_2: rutile TiO_2 (Entry 3: the R-TiO_2 support for Pt was a mixed phase of 20% rutile and 80% anatase).

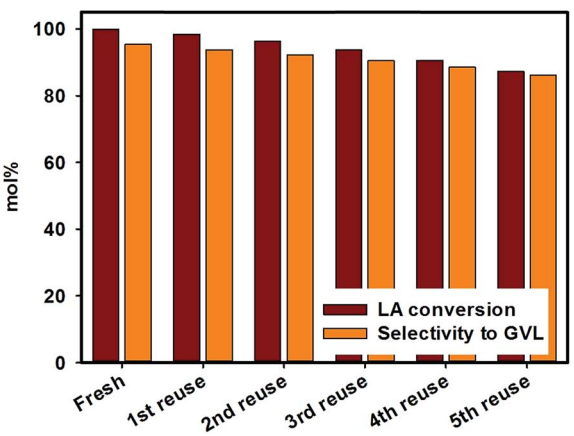

Fig. 7 LA conversion and GVL selectivity after 4 h reaction in the presence of 1% Pt@TiO_2 and AAB co-catalyst (fresh and consecutive hydrogenation cycles of the spent catalyst).

We also examined hydrogenation of furfural to furfuryl alcohol, an important industrial chemical intermediate and possible formation of reaction side-products such as tetrahydrofurfuryl alcohol (THFA) and 2-methylfuran (2-MF) over 1% Pt@TiO_2 and 1% Pt@TiO_2 in combination with AAB co-catalyst. The resultant 1% Pt@TiO_2 and combined 1% Pt@TiO_2 and AAB co-catalyst both display good catalytic performance with actual yields of furfuryl alcohol of 33.3% (65.7% selectivity at 50.7% conversion) in the case of 1% Pt@TiO_2 and 45.4% (68.4% selectivity at 66.4% conversion) in the case of 1% Pt@TiO_2 with AAB co-catalyst for 240 min reaction at 413.2 K. The favorable formation of furfuryl alcohol from hydrogenation of furfural in water has been recently reported by Li and his group[49] in the presence of Pd@C and Amberlyst™ 70 dual catalysts. Details of the effects of reaction time and temperature on the conversion and selectivity toward furfuryl alcohol in the hydrogenation of furfural over 1% Pt@TiO_2 and 1% Pt@TiO_2 in combination with AAB co-catalyst are not given because our study focused on the production of GVL as desirable end product.

Conclusions

We demonstrate herein a green approach for production of GVL from sugarcane bagasse involving a first step for hydrothermal conversion of biomass to LA and a second step for catalytic hydrogenation of LA to GVL; both steps worked in a green solvent such as water. The temperature variation experiments in the hydrothermal conversion step showed an upward trend of cellulose and hemicellulose conversion with reaction temperature; however LA yields did not follow the same trend. A very low amount of LA was detected in the reaction product mixture from non-catalyzed hydrothermal reaction, which was attributed to incomplete, slow and non-selective conversion of cellulose in pure sub-CW medium. It has been demonstrated that the presence of heterogeneous solid acid catalyst having strong Bronsted and Lewis acidity such as acid-activated bentonite increases not only the hydrothermal degradation rates of cellulose and hemicellulose into monosaccharides, but also favors the formation of furan ring-opening products such as LA.

The TiO_2-supported platinum metal (Pt@TiO_2) in combination with acid-activated bentonite as a co-catalyst was utilized in the catalytic hydrogenation of LA to GVL under moderate temperatures. It was found that the presence of acid-activated bentonite co-catalyst could improve the reaction rate while maintaining high selectivity toward GVL, thus enabling the adoption of even milder conditions to perform the reaction. Recyclability study showed that the spent 1% Pt@TiO_2 combined with AAB co-catalyst could retain its catalytic performance up to five consecutive hydrogenation cycles. Catalyst poisoning was primarily caused by coke deposition on the active catalyst sites, presumably from the polymerization of ALs over solid AAB surface.

Acknowledgements

J. N. Putro would like to express her sincere appreciation to the department of chemical engineering, National Taiwan University of Science and Technology (NTUST) for providing all the research facilities under the undergraduate internship program. The partial financial support from the Directorate General of Higher Education (DIKTI) through Undergraduate Student Research Grant Programs is also gratefully acknowledged.

References

1 R. E. H. Sims, W. Mabee, J. N. Saddler and M. Taylor, *Bioresour. Technol.*, 2010, **101**, 1570–1580.
2 G. W. Huber, S. Iborra and A. Corma, *Chem. Rev.*, 2006, **106**, 4044–4098.
3 S. Liu, L. P. Abrahamson and G. M. Scott, *Biomass Bioenergy*, 2012, **39**, 1–4.
4 H. Schwaiger, A. Tuerk, N. Pena, J. Sijm, A. Arrasto and C. Kettner, *Biomass Bioenergy*, 2012, **38**, 102–108.
5 J. Wang, J. Xi and Y. Wang, *Green Chem.*, 2015, **17**, 737–751.
6 S. W. Fitzpatrick, Production of levulinic acid from carbohydrate-containing materials, *US Pat.*, 5608105, Biofine Incorporated, March 04 1997.
7 S. S. Toor, L. Rosendahl and A. Rudolf, *Energy*, 2011, **36**, 2328–2342.
8 K. Yan and A. Chen, *Energy*, 2013, **58**, 357–363.
9 J. M. Tukacs, R. V. Jones, F. Darvas, G. Dibo, G. Lezsak and L. T. Mika, *RSC Adv.*, 2013, **3**, 16283–16287.
10 K. Shimizu, S. Kanno and K. Kon, *Green Chem.*, 2014, **16**, 3899–3903.
11 A. V. Bridgwater, *Catal. Today*, 1996, **29**, 285–295.
12 M. Selva, M. Gottardo and A. Perosa, *ACS Sustainable Chem. Eng.*, 2013, **1**, 180–189.
13 S. G. Wettstein, J. Q. Bond, D. M. Alonso, H. N. Pham, A. K. Datye and J. A. Dumesic, *Appl. Catal., B*, 2012, **117–118**, 321–329.
14 O. A. Abdelrahman, A. Heyden and J. Q. Bond, *ACS Catal.*, 2014, **4**, 1171–1181.
15 K. Yan and A. Chen, *Fuel*, 2014, **115**, 101–108.
16 W. R. H. Wright and R. Palkovits, *ChemSusChem*, 2012, **5**, 1657–1667.
17 A. M. Hengne and C. V. Rode, *Green Chem.*, 2012, **14**, 1064–1072.
18 X. L. Du, Q. Y. Bi, Y. M. Liu, Y. Cao and K. N. Fan, *ChemSusChem*, 2011, **4**, 1838–1843.
19 F. M. A. Geilen, B. Engendahl, M. Holscher, J. Klankermayer and W. Leitner, *J. Am. Chem. Soc.*, 2011, **133**, 14349–14358.
20 W. Li, J. H. Xie, H. Lin and Q. L. Zhou, *Green Chem.*, 2012, **14**, 2388–2390.
21 J. M. Tukacs, M. Novak, G. Dibo and L. T. Mika, *Catal. Sci. Technol.*, 2014, **4**, 2908–2912.
22 I. T. Horvath, H. Mehdi, V. Fabos, L. Boda and L. T. Mika, *Green Chem.*, 2008, **10**, 238–242.
23 L. Qi, Y. F. Mui, S. W. Lo, M. Y. Lui, G. R. Akien and I. T. Horvath, *ACS Catal.*, 2014, **4**, 1470–1477.
24 A. Stradi, M. Molnar, M. Ovari, G. Dibo, F. U. Richter and L. T. Mika, *Green Chem.*, 2013, **15**, 1857–1862.
25 M. Chalid, H. J. Heeres and A. A. Broekhuis, *J. Appl. Polym. Sci.*, 2012, **123**, 3556–3564.
26 L. Hu, G. Zhao, W. Hao, X. Tang, Y. Sun, L. Lin and S. Liu, *RSC Adv.*, 2012, **2**, 11184–11206.
27 G. Novodarszki, N. Retfalvi, G. Dibo, P. Mizsey, E. Csefalvay and L. T. Mika, *RSC Adv.*, 2014, **4**, 2081–2088.
28 G. R. Akien, L. Qi and I. T. Horvath, *Chem. Commun.*, 2012, **48**, 5850–5852.
29 F. E. Soetaredjo, A. Ayucitra, S. Ismadji and A. L. Maukar, *Appl. Clay Sci.*, 2011, **53**, 341–346.
30 C. Zhang, H. He and K. Tanaka, *Appl. Catal., B*, 2006, **65**, 37–43.
31 H. Yang, R. Yan, H. Chen, D. H. Lee and C. Zheng, *Fuel*, 2007, **86**, 1781–1788.
32 M. Garcia-Perez, A. Chaala, J. Yang and C. Roy, *Fuel*, 2001, **80**, 1245–1258.
33 S. Cao and G. M. Aita, *Bioresour. Technol.*, 2013, **131**, 357–364.
34 P. J. du Toit, S. P. Olivier and P. L. van Biljon, *Biotechnol. Bioeng.*, 1984, **26**, 1071–1078.
35 H. Yu, W. Du, J. Zhang, F. Ma, X. Zhang and W. Zhong, *Bioresour. Technol.*, 2010, **101**, 6728–6734.
36 S. Kim and M. T. Holtzapple, *Bioresour. Technol.*, 2005, **96**, 1994–2006.
37 D. A. Salvi, G. M. Aita, D. Robert and V. Bazan, *Appl. Biochem. Biotechnol.*, 2010, **161**, 67–74.
38 R. A. Silverstein, Y. Chen, R. R. Sharma-Shivappa, M. D. Boyette and J. Osborne, *Bioresour. Technol.*, 2007, **98**, 3000–3011.
39 R. Gupta and Y. Y. Lee, *Bioresour. Technol.*, 2010, **101**, 8185–8191.
40 Z. Yu, H. Jameel, H. M. Chang and S. Park, *Bioresour. Technol.*, 2011, **102**, 9083–9089.
41 Y. S. Cheng, Y. Zheng, C. W. Yu, T. M. Dooley, B. M. Jenkins and J. S. VanderGheynst, *Appl. Biochem. Biotechnol.*, 2010, **162**, 1768–1784.
42 C. Falco, N. Baccile and M. M. Titirici, *Green Chem.*, 2011, **13**, 3273–3281.
43 D. Doulia, C. Leodopoulos, K. Gimouhopoulos and F. Rigas, *J. Colloid Interface Sci.*, 2009, **340**, 131–141.
44 A. Onda, T. Ochi and K. Yanagisawa, *Green Chem.*, 2008, **10**, 1033–1037.

45 M. Moonsiri, P. Rangsunvigit, S. Chavadej and E. Gulari, *Chem. Eng. J.*, 2004, **97**, 241–248.
46 Y. Yu, X. Lou and H. Wu, *Energy Fuels*, 2008, **22**, 46–60.
47 J. N. Chheda, Y. Roman-Leshkov and J. A. Dumesic, *Green Chem.*, 2007, **9**, 342–350.
48 B. F. M. Kuster, *Starch-Starke*, 1990, **42**, 314–321.
49 X. Hu, R. J. M. Westerhof, L. Wu, D. Dong and C. Z. Li, *Green Chem.*, 2015, **17**, 219–224.
50 J. Jow, G. L. Rorrer, M. C. Hawley and D. T. A. Lamport, *Biomass*, 1987, **14**, 185–194.
51 P. L. Dhepe and R. Sahu, *Green Chem.*, 2010, **12**, 2153–2156.
52 C. Moreau, R. Durand, S. Razigade, J. Duhamet, P. Faugeras, P. Rivalier, P. Ros and G. Avignon, *Appl. Catal., A*, 1996, **145**, 211–224.
53 R. Weingarten, G. A. Tompsett, W. C. Conner Jr and G. W. Huber, *J. Catal.*, 2011, **279**, 174–182.
54 E. Nikolla, Y. Roman-Leshkov, M. Moliner and M. E. Davis, *ACS Catal.*, 2011, **1**, 408–410.
55 J. Wang, J. Ren, X. Liu, J. Xi, Q. Xia, Y. Zu, G. Lu and Y. Wang, *Green Chem.*, 2012, **14**, 2506–2512.
56 A. J. Crisci, M. H. Tucker, M. Y. Lee, S. G. Jang, J. A. Dumesic and S. L. Scott, *ACS Catal.*, 2011, **1**, 719–728.
57 M. Watanabe, Y. Aizawa, T. Iida, T. M. Aida, C. Levy, K. Sue and H. Inomata, *Carbohydr. Res.*, 2005, **340**, 1925–1930.
58 S. S. Joshi, A. D. Zodge, K. V. Pandare and B. D. Kulkarni, *Ind. Eng. Chem. Res.*, 2014, **53**, 18796–18805.
59 F. Chambon, F. Rataboul, C. Pinel, A. Cabiac, E. Guillon and N. Essayem, *Appl. Catal., B*, 2011, **105**, 171–181.
60 B. Tyagi, C. D. Chudasama and R. V. Jasra, *Spectrochim. Acta, Part A*, 2006, **64**, 273–278.
61 D. S. Tong, X. Xia, X. P. Luo, L. M. Wu, C. X. Lin, W. H. Yu, C. H. Zhou and Z. K. Zhong, *Appl. Clay Sci.*, 2013, **74**, 147–153.
62 J. S. Kruger, V. Nikolakis and D. G. Vlachos, *Curr. Opin. Chem. Eng.*, 2012, **1**, 312–320.
63 J. C. Serrano-Ruiz, R. M. West and J. A. Dumesic, *Annu. Rev. Chem. Biomol. Eng.*, 2010, **1**, 79–100.
64 P. P. Upare, J. M. Lee, D. W. Hwang, S. B. Halligudi, Y. K. Hwang and J. S. Chang, *J. Ind. Eng. Chem.*, 2011, **17**, 287–292.
65 A. Primo, P. Concepcion and A. Corma, *Chem. Commun.*, 2011, **47**, 3613–3615.
66 A. M. Ruppert, J. Grams, M. Jedrzejczyk, J. Matras-Michalska, N. Keller, K. Ostojska and P. Sautet, *ChemSusChem*, 2015, DOI: 10.1002/cssc.201403332.
67 J. P. Lange, R. Price, P. M. Ayoub, J. Louis, L. Petrus, L. Clarke and H. Gosselink, *Angew. Chem., Int. Ed.*, 2010, **49**, 4479–4483.
68 A. M. R. Galletti, C. Antonetti, V. De Luise and M. Martinelli, *Green Chem.*, 2012, **14**, 688–694.
69 Z. P. Yan, L. Lin and S. Liu, *Energy Fuels*, 2009, **23**, 3853–3858.
70 Y. Sarikaya, M. Onal, B. Baran and T. Alemdaroglu, *Clays Clay Miner.*, 2000, **48**, 557–562.